Modeling deep brain stimulation evoked responses with phase oscillator networks

Jonathan Realmuto*, Jessica Vidmark*, and Terence Sanger

***Abstract*— Deep brain stimulation is a highly effective therapy for an increasing number of neurological and psychiatric disorders. However, the optimal electrode placement and stimulation parameters are not the same for each individual and thus careful planning and tuning is required. The process can be time-consuming and usually heuristically guided by clinician experience. Personalized models tuned for each individual that capture important features of the underlying network dynamics would provide a quantitative method for target localization and stimulation tuning. Towards this, we present a preliminary investigation on modeling deep brain evoked responses with a network phase oscillator model. The model provides a forward dynamic simulation with the stimulation signal as input and average response of each subpopulation as output. The parameters of the model include the coupling strength within and between subpopulations and the topology of the network. We train the model using averaged data from a pediatric primary dystonia patient during a burst stimulation protocol in the globus pallidum. Our model provides a good fit to the data with an R-squared of 0.80. Using a contrasting data set with different stimulation parameters, we show our model provides a similar response suggesting it captures important features of the network dynamics.**

I. Introduction

Deep brain stimulation (DBS) has emerged as an important treatment paradigm for a variety of neurological and psychiatric disorders, including Parkinson's disease, essential tremor, dystonia, obsessive-compulsive disorder, depression, and epilepsy [1]. DBS involves the placement of a neurostimulator to generate electrical impulses through implanted electrodes to stimulate specific targets in the brain, typically structures in the basal ganglia and thalamus. The electrodes can also be used to directly measure brain activity. A typical intervention requires analysis of the patient's physiology and etiology, planning of the DBS targets, and, after implantation, careful tuning of the stimulation parameters. Predicting the responses to different stimulation targets and parameters would aid clinicians in target selection and parameter optimization, and is therefore of critical clinical significance.

Evoked oscillatory neural responses (EONR) have recently been observed in Parkinson's disease (PD) in the subthalamic nucleus (STN) and globus pallidus (GP) during STN stimulation [2]–[5]. The mechanism responsible for this behavior remains unclear with some proposed theories involving patterns of inhibition and excitation [6] and interactions between STN and connected structures, such as the pallidum [7], [8]. The EONR is a promising biomarker that could guide in electrode implantation surgery, locate the most effective stimulation contacts post-implantation, and provide a feedback signal for closed-loop DBS [3], [5].

We have observed a similar phenomenon in a primary dystonic patient localized around STN and ventral oralis (VO), with a smaller response observed in ventral intermediate (VIM), during GPi stimulation. These responses share many of features as previously reported EONRs in PD patients, including the stereotyped "resonant" response, where the amplitude increases and sharpens across consecutive pulses, the amplitude range, and the latency till peak-response.

Our aim here is to explore a network phase oscillator model for use in forward dynamic simulations of DBS. Phase oscillator models, typically abstracted in the form of the famed Kuramoto oscillator [9], provide the mathematical framework for collective synchronization and phase transitions [10], and have been used to describe feedback loops between excitation and inhibition in large neuronal networks [11], explain neuronal inhibition in DBS [12], described phase-locking mechanisms in DBS [13], and to replicate empirical relationships of cortical oscillations [14]. We introduce a new multi-population phase oscillator network, trained on empirical EONR, to realize a forward dynamic simulation of the underlying network, and subsequently probe the model with a different set of stimulation parameters.

II. Computational Methods

A. Model Overview

Our model is a variation of the Kuramoto phase oscillator [9] and includes positive and negative coupling [15] and interactions between subpopulations [16]. The coupling strength parameter models excitatory (positive values) and inhibitory (negative values) interactions. Excitatory interactions tend to synchronize, while inhibitory interactions tend to desynchronize. We partition the network into distinct subpopulations, each one modeling a specific target in the deep brain, and each consisting of an equal number of phase oscillator. The subpopulation influences the other subpopulations through network interactions (projections), e.g., directed connections between the oscillators of one subpopulation to the oscillators of another subpopulation. We restrict the coupling strength to be the same for the connections within each subpopulation and for of the subpopulation-to-subpopulation connections. Lastly, to model the DBS stimulation, we allow

*These authors contributed equally.

J. Realmuto is with the Department of Mechanical Engineering, University of California, Riverside. jrealmut@ucr.edu

J. Vidmark is with the Department of Biomedical Engineering, University of California, Irvine. jvidmark@uci.edu

T. Sanger is with Children's Hospital of Orange Country, and with the Department of Electrical Engineering and Computer Science, and the School of Medicine, University of California, Irvine. terry@sangerlab.net

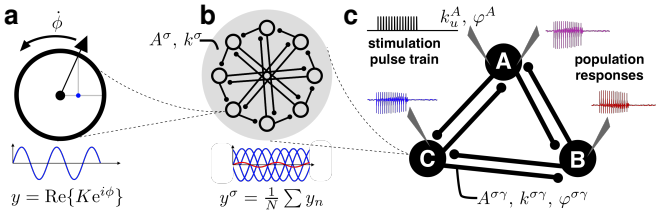

Fig. 1. Details of the proposed phase oscillator network model. **a** Each oscillator emits a sinusoidal responses y with phase ϕ and amplitude K. The phase dynamics $\dot{\phi}$ evolve according to Eq. (1). **b** Each subpopulation σ consists of N oscillators interacting according to the adjacency matrix A^σ with coupling strength k^σ. The total response y^σ of subpopulation σ is the average oscillator response over all oscillators with the subpopulation. **c** We consider three subpopulations (A, B, and C) influencing each other with subpopulation-to-subpopulation adjacency matrices $A^{\sigma\gamma}$, coupling strength $k^{\sigma\gamma}$, and phase shift $\varphi^{\sigma\gamma}$. The oscillators in subpopulation A are coupled to the stimulation with coupling strength k_u^A and phase φ^A.

for coupling with the stimulation pulses through a final coupling parameter. A summary of the multi-scale model is provided in Fig. 1. The phase dynamics of the n^{th} node within subpopulations σ is

$$\begin{aligned}\dot{\phi}_n^\sigma = \ & \omega^\sigma - k^\sigma \sum_{m=1}^{N} A_{nm}^\sigma \sin(\phi_n^\sigma - \phi_m^\sigma) \\ & - \sum_{\gamma\in\mathcal{N}_\sigma} k^{\sigma\gamma} \sum_{m=1}^{N} A_{nm}^{\sigma\gamma} \sin(\phi_n^\sigma - \phi_m^\gamma + \varphi^{\sigma\gamma}) \\ & - k_u^\sigma \sin(\phi_n^\sigma + \varphi^\sigma) u \end{aligned} \tag{1}$$

where ϕ_n^σ is the phase of the n^{th} oscillator within the subpopulation σ, ω^σ is subpopulation σ's natural frequency, k^σ is the local coupling strength within the subpopulation, N is the number of oscillators in the subpopulation, A^σ is the local network adjacency matrix, $\mathcal{N}_\sigma$ is the set of subpopulations that have projections onto subpopulation σ, $k^{\sigma\gamma}$ is the projection coupling strength of subpopulation γ onto subpopulation σ, $A^{\sigma\gamma}$ is the network adjacency matrix of subpopulation γ onto subpopulation σ, $\varphi^{\sigma\gamma}$ is the constant phase shift between the oscillator in subpopulation σ and the oscillators in subpopulation γ, k_u^σ is the coupling strength of subpopulation σ and the DBS stimulation, φ^σ is the constant phase shift between the DBS stimulation and the oscillators in subpopulation σ, and u is the stimulation signal, which in practice is a binary signal encoding the stimulation pulses. The connectivity within and between each subpopulation is encoded using directed adjacency matrices whose elements are $A_{nm} = 1$ for a connection (interaction) from oscillators m to n. The output of each oscillator is sinusoidal, and the response of each subpopulation is the average response over all subpopulation oscillators:

$$y^\sigma = \frac{1}{N}\sum_{n=1}^{N} \mathrm{Re}\{Ke^{i\phi_n^\sigma}\}. \tag{2}$$

with $i = \sqrt{-1}$, K the amplitude, and $\mathrm{Re}\{\cdot\}$ the real part.

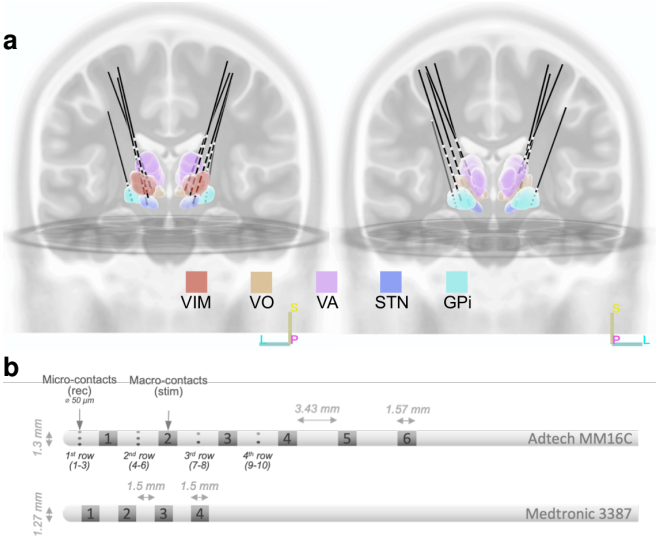

Fig. 2. **a** Front (left) and back (right) views of the DBS lead implant locations. White portions on the black leads represent the low-impedance macro contacts. The image was generated by normalizing a post-operative computed tomography scan onto a pre-operative magnetic resonance imaging scan, in combination with regions of interest from an adult template. Acronyms: globus pallidus interna (GPi), ventral intermediate (VIM), subthalamic nucleus (STN), ventral oralis (VO). **b** Detailed schematic of the two types of electrodes implanted. Top: Adtech electrodes used as the temporary electrodes. Bottom: Medtronic electrodes used permanently and the electrodes that were previously implanted in the participant.

B. Network Topology

The network topology was designed through preliminary investigations and we sought a responsive and highly coupled network, but without all-to-all connections which are computationally expensive. Starting with a directed ring network, where the oscillators of each subpopulation are arranged in a ring and each project to one neighbor (e.g., counterclockwise neighbor), we found that this often resulted in chimera states [17], where clusters of oscillators will synchronize together, even if the local coupling parameter is negative (desynchronizing), but out of phase with other clusters. To avoid this behavior, we added a second projection from each oscillator to its farthest neighbor. The final network design can be seen in Fig. 1**b** and is described by

$$\bar{A}_{nm} = \begin{cases} 1 \text{ if } m = (n+1) \bmod N \text{ or } m = \frac{n+N}{2} \bmod N \\ 0 \end{cases} \tag{3}$$

In this work, the network connections all take this form: $A^\sigma = A^{\sigma\gamma} = \bar{A}$, $\forall\gamma \in \mathcal{N}_\sigma$, for each subpopulation σ.

C. Model Setup and Optimization Procedure

The number of subpopulations were chosen to replicate the empirical recordings, which are described in detail in the next section, and thus includes three subpopulations ($\sigma \in \{A, B, C\}$), corresponding to the target structures GPi, VIM, and VO/STN (see Fig. 1**c**). Each subpopulation had $N = 8$ oscillators. Only subpopulation A (GPi) is allowed stimulation coupling with strength parameter k_u^A. The constant phase delays were assumed to be symmetric,

so that $\varphi^{\sigma\gamma} = \varphi^{\gamma\sigma}$. Given these assumptions, there were 18 parameters fitted to the empirical data. The parameters where optimized via minimizing the following cost function

$$J = \sum_{t\in\mathcal{T}} (y^{\text{GPi}}(t) - y^{A}(t))^2 + (y^{\text{VIM}}(t) - y^{B}(t))^2 + (y^{\text{VO}}(t) - y^{C}(t))^2 \quad (4)$$

which is the squared error taken only during the EONR activity, parameterized by the set $\mathcal{T}$, e.g., an index mask that identifies the regions of interests. Since the problem is non-convex, with many local minima, we alternated between a gradient based solver (`fmincon` in Matlab) and a derivative-free search (`patternsearch` in Matlab). All simulations are numerically integrated using a first order Euler method with a time step matching the sampling frequency of the processed data.

III. Experimental Methods

A. Patient Selection

The participant for clinical DBS surgery was chosen based on the inclusion criteria of all of the following: presence of movement disorder, significantly limiting or interfering with normal function or care; potential stimulation targets, identifiable with magnetic resonance imaging; and low success from symptomatic or etiologic medical therapy. Prior to the study, the participant's legal guardians provided HIPAA authorization for research use of protected health information, as well as written informed consent, both for surgical procedures conforming to standard hospital practice, and for research use of electrophysiological data. All research use of data was approved by the institutional review board of Children's Hospital of Orange County (CHOC). Data from 1 pediatric patient (female, 16 years old) with primary dystonia (DYT1) was used in this case study.

B. Electrode Placement

Seven temporary Adtech MM16C depth electrodes (Adtech Medical Instrument Corp., Oak Creek, WI, USA; Fig. 2**a**) were implanted into potential DBS targets, identified prior to surgery through a collaborative consultation between the departments of Neurology and Neurosurgery at CHOC. Target areas were in the thalamus (ventral intermediat (VIM), ventral anterior (VA), and ventral oralis, (VO)) and basal ganglia (globus pallidus internal (GPi), and subthalamic nucleus (STN). Each implanted electrode consisted of 6 low-impedance macro-contacts, and 10 high-impedance micro-contacts. These intracranial electrodes were linked to amplifier inputs via Adtech Cabrio connectors, through shielded cables. The patient studied in this paper also had previously implanted permanent leads consisting of 4 macro-contacts (Medtronic 3387) bilaterally in GPi. The electrode schematics are provided in Fig. 2**b**.

C. Stimulation Parameters and Data Acquisition

Experiments were conducted during the period 2-5 days following the electrode implantation after the patient fully recovered from general anesthesia. Stimulations consisted of passive charge-balanced 3.5 Volt 150 Hz pulses with a 5 Hz burst frequency (100 millisecond of stimulations separated by 100 milliseconds without stimulation). The stimulations were applied bilaterally, with 180-degree phase shift in timing, in the permanent GPi leads with 120 microsecond pulse width through contacts 0-1+ in the left hemisphere and 60 microsecond pulses through contacts 0-Case+ in the right hemisphere. Twenty seconds of concurrent bilateral stimulation were performed, generating approximately 100 stimulation bursts. The second stimulation protocol consisted of the same stimulation parameters, except with constant (not bursts) of 185 Hz pulses and the data includes 1000 cycles. All data was recorded concurrently during through all micro-contacts with a sampling frequency of 22 kHz and subsequently bandpass filtered at 0.3-9 KHz. The recordings were digitized and written to a hard drive using a PZ5M Medically Isolated NeuroDigitize, RZ2 Bioamp processor, and RS4 Data Streamer (Tucker-Davis Technologies Inc., Alachua, FL, USA).

D. Data Post Processing

In this study, we analysed the stimulation and responses from the right hemisphere. The neural activity was taken as the relative response between two nearby electrodes (local bipolar recordings). All segments were aligned through cross-correlation of the last artefact in the stimulation burst. The approximately 100 stimulation bursts were then averaged across each time point. The stimulation artefacts were identified [18], and the index mask (e.g., $\mathcal{T}$ in Eq. (4)) was determined as the time span after an artifact till the index before the start of the subsequent pulse. Next, independent component analysis (ICA) was used for source separation. The ICA procedure was conducted independently for each electrode (eight bipolar channels per electrode were selected for ICA). After ICA, the signals were centered to have zero mean and were visual inspected, with the channel from the followint electrodes chosen based on the amplitude and clarity of the response as the ground truth for the model training: GPi, VIM, and VO/STN. Note that the VO/STN electrode spans both structures.

IV. Results and Discussion

The forward dynamic simulation, after model optimization, provides a remarkably similar response when compared with the empirical data, as can been seen by comparing Fig. 3**a** & **b** with **c** & **d**. The model adequately captures the EONRs, including the "resonant" behavior, where the amplitude increases and sharpens with consecutive stimulation pulses, and captures the "ringing" effect after the last cycle. With an R-squared value of 0.8, our model explains a large portion of the variance within the original data. Using the same optimized model parameters, we simulated a second set of empirical data, where the stimulation was held constant (not bursts) at 185 Hz. The original data is shown in Fig. 3**e** & **f** and the simulation is shown in Fig. 3**g** & **h**. Note that in neither the model nor the data is there an EONR apparent for the 185 Hz stimulation.

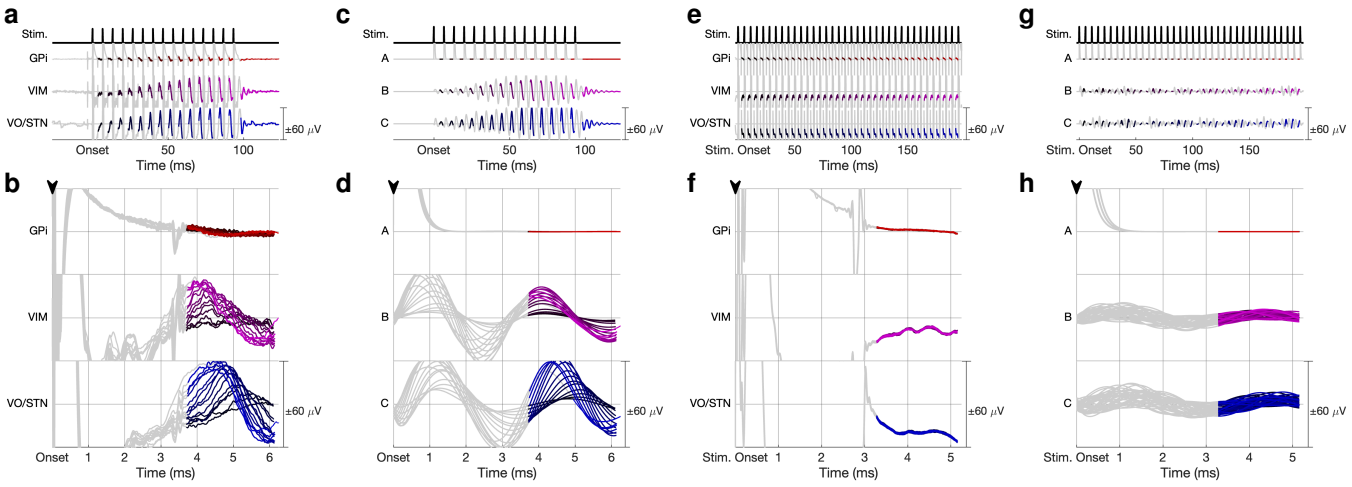

Fig. 3. Comparison of the empirical data and simulations. **a** Empirical response during 150 Hz burst stimulation. Colored portions of the traces represent the regions of interest, e.g., the EONRs. **b** Superimposed EONRs aligned to each pulse (time is encoded in trace shading, darker to lighter shades). **c** Simulated response of the 150 Hz stimulation. **d** Simulated EONRs aligned to each pulse. **e** Empirical response during 185 Hz stimulation. **f** Superimposed responses aligned to pulse. **c** Simulated response of the 185 Hz stimulation. **d** Simulation responses aligned to each pulse. (The stimulation artifact from the contralateral stimulations, which were phase shifted by 180 degrees relative to the ipsilateral stimulation, can be seen in the two empirical data sets, at the 3.33 millisecond mark in **b**, and 2.70 millisecond mark in **f**.)

V. Conclusion

We introduced a network phase oscillator model for dynamic simulations of DBS. Using empirical data, most likely related to a recently discover biomarker, we showed that the parameters of the model could be optimized to produce a remarkably similar forward dynamic simulation, resulting in a good model fit to the empirical data (R-squared = 0.80). Using a second empirical data set, which was generated under different stimulation conditions, we showed that our model provides reasonable agreement with the data, suggesting the model captures important features of the individual neural network. Our results suggest phase oscillator model should be further investigated for potential applications in model-based DBS.

References

[1] A. M. Lozano, N. Lipsman, H. Bergman, P. Brown, S. Chabardes, J. W. Chang, K. Matthews, C. C. McIntyre, T. E. Schlaepfer, M. Schulder *et al.*, "Deep brain stimulation: current challenges and future directions," *Nature Reviews Neurology*, vol. 15, no. 3, pp. 148–160, 2019.

[2] N. C. Sinclair, H. J. McDermott, K. J. Bulluss, J. B. Fallon, T. Perera, S. S. Xu, P. Brown, and W. Thevathasan, "Subthalamic nucleus deep brain stimulation evokes resonant neural activity," *Annals of neurology*, vol. 83, no. 5, pp. 1027–1031, 2018.

[3] N. C. Sinclair, H. J. McDermott, J. B. Fallon, T. Perera, P. Brown, K. J. Bulluss, and W. Thevathasan, "Deep brain stimulation for parkinson's disease modulates high-frequency evoked and spontaneous neural activity," *Neurobiology of disease*, vol. 130, p. 104522, 2019.

[4] C. Wiest, G. Tinkhauser, A. Pogosyan, M. Bange, M. Muthuraman, S. Groppa, F. Baig, A. Mostofi, E. Pereira, H. Tan *et al.*, "Local field potential activity dynamics in response to deep brain stimulation of the subthalamic nucleus in parkinson's disease," *Neurobiology of disease*, vol. 143, p. 105019, 2020.

[5] S. L. Schmidt, D. T. Brocker, B. D. Swan, D. A. Turner, and W. M. Grill, "Evoked potentials reveal neural circuits engaged by human deep brain stimulation," *Brain stimulation*, vol. 13, no. 6, pp. 1706–1718, 2020.

[6] W. Meissner, A. Leblois, D. Hansel, B. Bioulac, C. E. Gross, A. Benazzouz, and T. Boraud, "Subthalamic high frequency stimulation resets subthalamic firing and reduces abnormal oscillations," *Brain*, vol. 128, no. 10, pp. 2372–2382, 2005.

[7] T. Hashimoto, C. M. Elder, M. S. Okun, S. K. Patrick, and J. L. Vitek, "Stimulation of the subthalamic nucleus changes the firing pattern of pallidal neurons," *Journal of neuroscience*, vol. 23, no. 5, pp. 1916–1923, 2003.

[8] G. Foffani and A. Priori, "Deep brain stimulation in parkinson's disease can mimic the 300 hz subthalamic rhythm," *Brain*, vol. 129, no. 12, pp. e59–e59, 2006.

[9] Y. Kuramoto, "Chemical turbulence," in *Chemical oscillations, waves, and turbulence*. Springer, 1984, pp. 111–140.

[10] S. H. Strogatz and R. E. Mirollo, "Stability of incoherence in a population of coupled oscillators," *Journal of Statistical Physics*, vol. 63, no. 3, pp. 613–635, 1991.

[11] E. Montbrió and D. Pazó, "Kuramoto model for excitation-inhibition-based oscillations," *Physical review letters*, vol. 120, no. 24, p. 244101, 2018.

[12] A. Franci, A. Chaillet, E. Panteley, and F. Lamnabhi-Lagarrigue, "Desynchronization and inhibition of kuramoto oscillators by scalar mean-field feedback," *Mathematics of Control, Signals, and Systems*, vol. 24, no. 1, pp. 169–217, 2012.

[13] G. Weerasinghe, B. Duchet, H. Cagnan, P. Brown, C. Bick, and R. Bogacz, "Predicting the effects of deep brain stimulation using a reduced coupled oscillator model," *PLoS computational biology*, vol. 15, no. 8, p. e1006575, 2019.

[14] T. Menara, G. Baggio, D. Bassett, and F. Pasqualetti, "Functional control of oscillator networks," *Nature communications*, vol. 13, no. 1, pp. 1–13, 2022.

[15] H. Hong and S. H. Strogatz, "Kuramoto model of coupled oscillators with positive and negative coupling parameters: an example of conformist and contrarian oscillators," *Physical Review Letters*, vol. 106, no. 5, p. 054102, 2011.

[16] E. Fengler, J. F. Totz, P. Kaluza, and H. Engel, "Directed adaptation of synchronization levels in oscillator communities," *Chaos: An Interdisciplinary Journal of Nonlinear Science*, vol. 29, no. 6, p. 063101, 2019.

[17] C. R. Laing, "The dynamics of chimera states in heterogeneous kuramoto networks," *Physica D: Nonlinear Phenomena*, vol. 238, no. 16, pp. 1569–1588, 2009.

[18] J. S. Vidmark, E. Hernandez-Martin, and T. D. Sanger, "Increasing consistency of evoked response in thalamic nuclei during repetitive burst stimulation of peripheral nerve in humans," in *International Conference on Medical Image Computing and Computer-Assisted Intervention*. Springer, 2021, pp. 238–247.